

## Theoretical Study of Spectral Responses of Homojunctions Based on CuInSe<sub>2</sub>

E.M. Keita\*, B. Mbow, M.S. Mane, M.L. Sow, C. Sow, C. Sene

Laboratoire des semiconducteurs et d'Energie solaire, Département de Physique, Faculté des Sciences et Techniques, Université Cheikh AntaDiop, Dakar, Sénégal.

### Article history

Received: 11-April-2016

Revised: 21-April-2016

Available online: 04-Aug-2016

### Keywords:

Thin films, CuInSe<sub>2</sub>, CuInS<sub>2</sub>, Internal quantum efficiency, Window layer and substrate effects

### Abstract

In this article we study the spectral responses of thin films solar cells based on CuInSe<sub>2</sub>. This is particularly important for the characterization of photoconductive layers. The objective is to compare the performances of the homojunction based on CuInSe<sub>2</sub> with a medium band gap window layer based on CuInS<sub>2</sub> according to the model CuInS<sub>2</sub>(p+)/CuInSe<sub>2</sub>(p)/CuInSe<sub>2</sub>(n), of the homojunction type CuInSe<sub>2</sub>(p)/CuInSe<sub>2</sub>(n) and the homojunction deposited on substrate type CuInSe<sub>2</sub>(p)/CuInSe<sub>2</sub>(n)/CuInSe<sub>2</sub>(n<sup>+</sup>). Calculation models of the internal quantum efficiency have been proposed for each structure. The comparison of these different results allows firstly to examine the influences of the window layer and the substrate, and secondly to optimize the photoelectrical parameters to enhance the global efficiency.

© 2016 JMSSE All rights reserved

### Introduction

The CuInSe<sub>2</sub> in its chalcopyrite form is a direct band gap semiconductor in the order of 1.04 eV [1-3] with a high photon absorption coefficient ( $\alpha > 10^5 \text{ cm}^{-1}$ ) [4-6], and present a great interest in solar applications [7,8]. With its high absorption coefficient, the photocarriers are created on a shallow thickness (1 to 2  $\mu\text{m}$ ). It results from this that the surface recombination velocity (a parameter which characterizes the surface of the semiconductor) and the junction depth effects are very important. Due to the disparity of the periodicity of the crystal lattice and of the adsorption of foreign atoms; the surface of the semiconductor is the seat of recombination [9]. The carriers lifetime in surface is therefore always less than to their lifetime in volume [9], this effect is characterized by a high surface recombination velocity. In order to reduce the losses of carriers on the surface, a window layer having a more elevated band gap and a neighbouring cell parameters to the active layer is often deposited on the surface of the latter [10]. The deposit of a substrate to the back surface also permits to reduce the losses of carriers on the back face and confine minority photocarriers in the base in order to increase their collections at the junction. However the window layer in case of high energies (energies values greater than the energy band gap of the window layer) and the substrate in case of low energies (depth absorption) can also have an important role in enhancing the efficiency of the solar cell in comparison with the homojunction.

In this work the models of cell used are the homojunction type CuInSe<sub>2</sub>(p)/CuInSe<sub>2</sub>(n), the homojunction with window layer type CuInS<sub>2</sub>(p+)/CuInSe<sub>2</sub>(p)/CuInSe<sub>2</sub>(n) and the homojunction deposited on a substrate type CuInSe<sub>2</sub>(p)/CuInSe<sub>2</sub>(n)/CuInSe<sub>2</sub>(n<sup>+</sup>). The CuInS<sub>2</sub> having a more wide band gap (in order of 1.57 eV) [11] than CuInSe<sub>2</sub>, can be used as a window layer for a limited range energy (1.04 eV to 1.57 eV), since these two materials belong to the same family (Cu-III-VI<sub>2</sub> group) [12] and have fairly similar

lattice parameters (see Table 1). The substrate doped n<sup>+</sup> and the base doped n are the same nature, the interface phenomena are neglected because there is a continuity of layers, then<sup>+</sup> doping allows to maintain photocarriers in the base (creating of a low barrier potential).

### Experimental

For each proposed structure, the theoretical model used for the determination of the spectral response is based on the effects of the absorption coefficients of the different materials and the geometrical and electrical parameters modeling the solar cell (diffusion length, recombination velocity at the front and the back surface and at the interface between different layers, thicknesses of the layers, etc.). It is assumed that the optical reflection coefficient is neglected at each interface in the spectral range used. It is also considered that the space charge region is located only between the p and n regions of each structure and there is no electric field outside this region. Moreover, in this same region, recombination phenomena are neglected.

The following **Table 1** lists the different physical parameters used in this work for each structure [11, 13 – 18]:

**Table 1:** Lists the different physical parameters used in this work for each structure

Material	E <sub>g</sub> (gap)	a	c	X (electron affinity)	Type (p,n)
CuInSe <sub>2</sub> (p,n)	0,96 – 1,04 eV	5,78 Å	11,62 Å	4,58 eV	10 <sup>14</sup> - 10 <sup>20</sup> cm <sup>-3</sup>
CuInS <sub>2</sub> (p)	1,438 - 1,57 eV	5,51 Å	11 Å	4,04 eV	10 <sup>16</sup> - 10 <sup>20</sup> cm <sup>-3</sup>

The absorption coefficients of the different materials (CuInSe<sub>2</sub> and CuInS<sub>2</sub>) used in this work is shown on figure 1. We used the values of the absorption coefficients given by Subba Ramaiah Kodigala [11] for photon energies ranging from 1 to 2 eV. We

have approximately completed these values for photon energies greater than 2 eV.

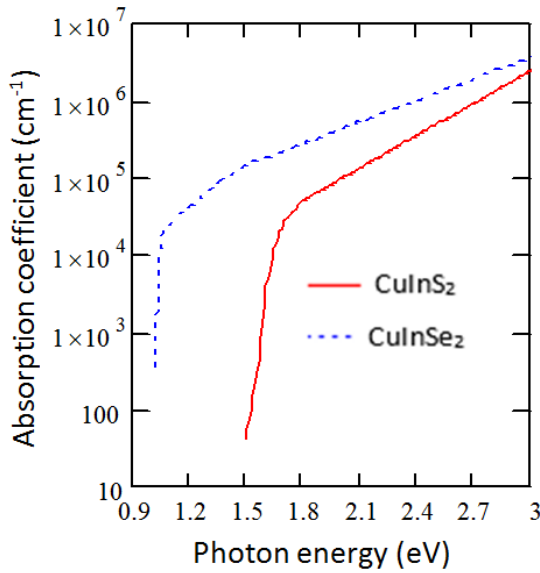


Figure 1: Absorption coefficient versus photon energy

**Three layers model type p<sup>+</sup>/p/n:homojunction with window layer type CuInS<sub>2</sub>(p<sup>+</sup>)/CuInSe<sub>2</sub>(p)/ CuInSe<sub>2</sub>(n)**

Homojunction type CuInSe<sub>2</sub>(p)/CuInSe<sub>2</sub>(n) is often characterized by losses of carriers by recombination at the front layer surface. To reduce surface phenomena, it is often deposited a window layer on the front surface, allowing to move away the surface to the active area. Therefore the surface of the front absorbent layer is replaced by the interface CuInS<sub>2</sub>(p<sup>+</sup>)/CuInSe<sub>2</sub>(n) having an enhanced quality because these two materials have some similar lattice parameters. The diagram of the structure is shown in Figure 2.

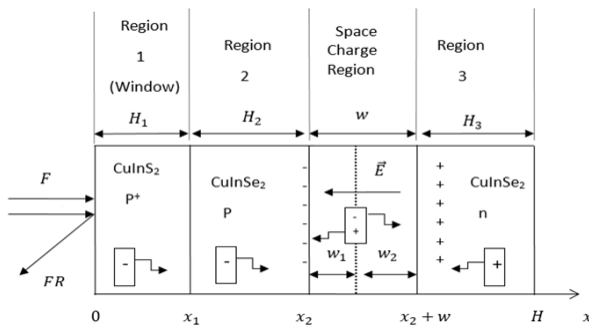


Figure 2: Diagram of the structure CuInS<sub>2</sub>(p<sup>+</sup>)/CuInSe<sub>2</sub>(p)/CuInSe<sub>2</sub>(n)

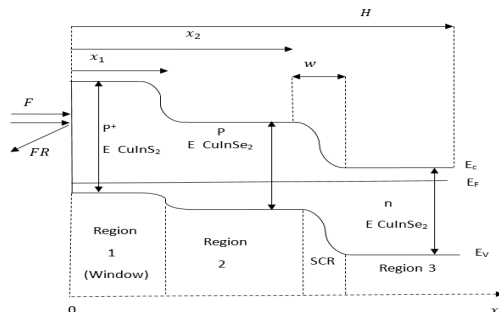


Figure 3: Energy band diagram of the structure CuInS<sub>2</sub>(p<sup>+</sup>)/CuInSe<sub>2</sub>(p)/CuInSe<sub>2</sub>(n)

The energy band diagram (Figure 3) is based on the Anderson model [19], it depend of electronic properties as the electron affinity, the width of the band gap and the doping level (see Table 1).

*Calculation of the photocurrent in region 1 (window layer)*

In region 1 (window layer), 0 ≤ x ≤ x<sub>1</sub>, the photocurrent is essentially due to the electrons, the continuity equation is:

$$\frac{d^2 \Delta n_1}{dx^2} - \frac{\Delta n_1}{L_{n_1}^2} = \frac{-\alpha_1 F(1-R)e^{-\alpha_1 x}}{D_{n_1}} \quad (2.1)$$

$$\text{With } L_{n_1}^2 = D_{n_1} \tau_{n_1} \quad (2.2)$$

We have the following boundary conditions [20]:

$$D_{n_1} \left( \frac{d\Delta n_1}{dx} \right) = S_{n_1} \Delta n_1 \quad \text{for } x = 0 \quad (2.3)$$

$$\Delta n_1 = 0 \quad \text{for } x = x_1 \quad (2.4)$$

The expression of the photocurrent is given by:

$$J_{n_1}(x_1) = -\frac{q\alpha_1 F(1-R)L_{n_1}}{(\alpha_1^2 L_{n_1}^2 - 1)} \left[ \frac{\left( \frac{S_{n_1} L_{n_1} + \alpha_1 L_{n_1}}{D_{n_1}} \right) e^{-\alpha_1 x_1} \left[ \frac{S_{n_1} L_{n_1} ch\left(\frac{x_1}{L_{n_1}}\right) + sh\left(\frac{x_1}{L_{n_1}}\right)}{\frac{S_{n_1} L_{n_1} sh\left(\frac{x_1}{L_{n_1}}\right) + ch\left(\frac{x_1}{L_{n_1}}\right)} - \frac{S_{n_1} L_{n_1} sh\left(\frac{x_1}{L_{n_1}}\right) + ch\left(\frac{x_1}{L_{n_1}}\right)}{D_{n_1}} \right]}{D_{n_1}} - \alpha_1 L_{n_1} e^{-\alpha_1 x_1} \right] \quad (2.5)$$

*Calculation of the photocurrent in Region 2*

In region 2, x<sub>1</sub> ≤ x ≤ x<sub>2</sub>, the photocurrent is also an electron current, it results from the contribution of the regions 1 and 2, taking into account the interface effect characterized by a recombination velocity at the interface noted S<sub>n<sub>2</sub></sub>. The continuity equation is given by:

$$\frac{d^2 \Delta n_2}{dx^2} - \frac{\Delta n_2}{L_{n_2}^2} = \frac{-\alpha_2 F(1-R)e^{-\alpha_1 x_1} e^{-\alpha_2(x-x_1)}}{D_{n_2}} \quad (2.6)$$

$$\text{With } L_{n_2}^2 = D_{n_2} \tau_{n_2} \quad (2.7)$$

The boundary conditions can be written by [21, 22]:

$$D_{n_2} \frac{d\Delta n_2}{dx} = S_{n_2} \Delta n_2 + D_{n_1} \frac{d\Delta n_1}{dx} \quad \text{for } x = x_1 \quad (2.8)$$

$$\Delta n_2 = 0 \quad \text{for } x = x_2 \quad (2.9)$$

The photocurrent expression is:

$$J_{n_2}(x_2) = -\frac{q\alpha_2 F(1-R)L_{n_2} e^{-\alpha_1 x_1}}{(\alpha_2^2 L_{n_2}^2 - 1)} \times \left\{ \frac{\left( \frac{S_{n_2} L_{n_2} + \alpha_2 L_{n_2}}{D_{n_2}} \right) e^{-\alpha_2(x_2-x_1)} \left[ \frac{S_{n_2} L_{n_2} ch\left(\frac{x_2-x_1}{L_{n_2}}\right) + sh\left(\frac{x_2-x_1}{L_{n_2}}\right)}{\frac{S_{n_2} L_{n_2} sh\left(\frac{x_2-x_1}{L_{n_2}}\right) + ch\left(\frac{x_2-x_1}{L_{n_2}}\right)} - \frac{S_{n_2} L_{n_2} sh\left(\frac{x_2-x_1}{L_{n_2}}\right) + ch\left(\frac{x_2-x_1}{L_{n_2}}\right)}{D_{n_2}} \right]}{D_{n_2}} - \alpha_2 L_{n_2} e^{-\alpha_2(x_2-x_1)} \right\} + \frac{J_{n_1}(x_1)}{\frac{S_{n_2} L_{n_2} sh\left(\frac{x_2-x_1}{L_{n_2}}\right) + ch\left(\frac{x_2-x_1}{L_{n_2}}\right)}{D_{n_2}}} \quad (2.10)$$

The first term of this expression corresponds to the photocurrent contributed by the region 2 itself and the second term is the contribution of region 1.

*Calculation of the photocurrent in Region 3*

In this region, x<sub>2</sub> + w ≤ x ≤ H, the photocurrent is a hole current, the continuity equation is:

$$\frac{d^2\Delta p_3}{dx^2} - \frac{\Delta p_3}{L_{p_3}^2} = \frac{-\alpha_3}{D_{p_3}} F(1-R)e^{-\alpha_1 x_1} \times e^{-\alpha_2[(x_2+w_1)-x_1]} e^{\alpha_3(x_2+w_1)} e^{-\alpha_3 x} \quad (2.11)$$

$$\text{With } L_{p_3}^2 = D_{p_3} \tau_{p_3} \quad (2.12)$$

The boundary conditions are given by[20]:

$$D_{p_3} \frac{d\Delta p_3}{dx} = -S_{p_3} \Delta p_3 \quad \text{for } x = H \quad (2.13)$$

$$\Delta p_3 = 0 \quad \text{for } x = x_2 + w \quad (2.14)$$

The holes photocurrent expression is:

$$J_{p_3}(x_2 + w) = \frac{q\alpha_3 L_{p_3} F(1-R)e^{[(\alpha_2-\alpha_1)x_1]} e^{[(\alpha_3-\alpha_2)(x_2+w_1)]}}{(\alpha_3^2 L_{p_3}^2 - 1)} \times \left\{ \frac{(\alpha_3 L_{p_3} - \frac{S_{p_3} L_{p_3}}{D_{p_3}}) e^{-\alpha_3 H}}{\frac{S_{p_3} L_{p_3}}{D_{p_3}} sh\left[\frac{H-(x_2+w)}{L_{p_3}}\right] + ch\left[\frac{H-(x_2+w)}{L_{p_3}}\right]} + e^{-\alpha_3(x_2+w)} \left\{ \frac{S_{p_3} L_{p_3}}{D_{p_3}} ch\left[\frac{H-(x_2+w)}{L_{p_3}}\right] + sh\left[\frac{H-(x_2+w)}{L_{p_3}}\right]} \frac{S_{p_3} L_{p_3}}{D_{p_3}} sh\left[\frac{H-(x_2+w)}{L_{p_3}}\right] + ch\left[\frac{H-(x_2+w)}{L_{p_3}}\right]} - \alpha_3 L_{p_3} e^{-\alpha_3(x_2+w)} \right\} \right\} \quad (2.15)$$

Neglecting the recombination of photocarriers, the photocurrent of electrons from the depletion regions is given by:

$$J_{n_{w_1}} = qF(1-R)e^{-\alpha_1 x_1} e^{-\alpha_2(x_2-x_1)} \times [e^{-\alpha_2 w_1} - 1] \quad (2.16)$$

$$J_{n_{w_2}} = qF(1-R)e^{-\alpha_1 x_1} \times e^{-\alpha_2[(x_2+w_1)-x_1]} \times [e^{-\alpha_3 w_2} - 1] \quad (2.17)$$

**Two layers model type p/n: homojunction type CuInSe<sub>2</sub>(p)/CuInSe<sub>2</sub>(n)**

To find results which are appropriate in the case of the homojunction, it is just sufficient to remove the window layer on Figures 1 and 2, and to establish  $x_1 = 0$  et  $\alpha_1 = 0$  in the expressions (2.10), (2.15), (2.16) and (2.17).

**Three layers model type p/n/n+: homojunction deposited on substrate type CuInSe<sub>2</sub>(p)/CuInSe<sub>2</sub>(n)/CuInSe<sub>2</sub>(n<sup>+</sup>)**

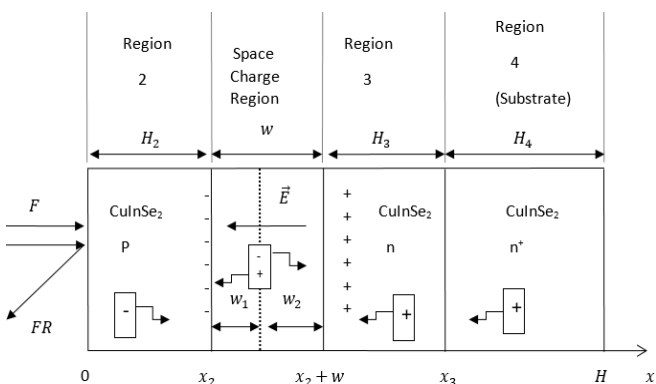


Figure 4: Diagram of the structure CuInSe<sub>2</sub>(p)/CuInSe<sub>2</sub>(n)/CuInSe<sub>2</sub>(n<sup>+</sup>)

The diagrams of the structure and the energy band are respectively shown in Figures 4 and 5.

The expressions of the electrons photocurrent in Region 2 and in the space charge region are identical to those established for the homojunction.

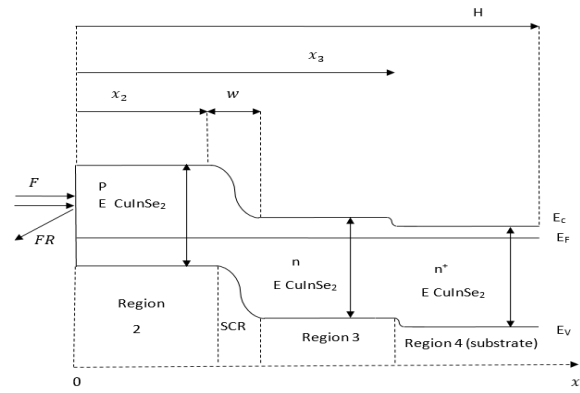


Figure 5: Energy band diagram of the structure CuInSe<sub>2</sub>(p)/CuInSe<sub>2</sub>(n)/CuInSe<sub>2</sub>(n<sup>+</sup>)

**Calculation of the holes photocurrent in regions 3 and 4**

The continuity equations in region 4 (substrate) and Region 3 (base) are respectively given by following equations (2-18) and (2-20) :

$$\frac{d^2\Delta p_4}{dx^2} - \frac{\Delta p_4}{L_{p_4}^2} = \frac{-\alpha_4}{D_{p_4}} F(1-R)e^{-\alpha_2[(x_2+w_1)]} \times e^{-\alpha_3[x_3-(x_2+w_1)]} e^{\alpha_4 x_3} e^{-\alpha_4 x} \quad (2.18)$$

$$\text{With } L_{p_4}^2 = D_{p_4} \tau_{p_4} \quad (2.19)$$

$$\frac{d^2\Delta p_3}{dx^2} - \frac{\Delta p_3}{L_{p_3}^2} = \frac{-\alpha_3}{D_{p_3}} F(1-R)e^{-\alpha_2[(x_2+w_1)]} \times e^{\alpha_3(x_2+w_1)} e^{-\alpha_3 x} \quad (2.20)$$

$$\text{With } L_{p_3}^2 = D_{p_3} \tau_{p_3} \quad (2.21)$$

The variation of the holes density in the substrate is given by the solution of equation (2-18), it is written as :

$$\Delta p_4(x) = A'_4 e^{x/L_{p_4}} + B'_4 e^{-x/L_{p_4}} + K'_{p_4} e^{-\alpha_4 x} \quad (2.22)$$

$$\text{With } K'_{p_4} = \frac{-\alpha_4 L_{p_4}^2 F(1-R)e^{[(\alpha_3-\alpha_2)(x_2+w_1)]} e^{[(\alpha_4-\alpha_3)x_3]}}{D_{p_4}(\alpha_4^2 L_{p_4}^2 - 1)} \quad (2.23)$$

The solution of the equation (2-20) gives the variation of the holes density in the base, it is written as:

$$\Delta p_3(x) = A'_3 e^{x/L_{p_3}} + B'_3 e^{-x/L_{p_3}} + K'_{p_3} e^{-\alpha_3 x} \quad (2.24)$$

$$\text{With } K'_{p_3} = \frac{-\alpha_3 L_{p_3}^2 F(1-R)e^{[(\alpha_3-\alpha_2)(x_2+w_1)]}}{D_{p_3}(\alpha_3^2 L_{p_3}^2 - 1)} \quad (2.25)$$

The constants  $A'_3$ ,  $B'_3$ ,  $A'_4$  et  $B'_4$  can be determined by establishing the following boundary conditions [23, 24]:

$$\Delta p_3(x) = 0 \quad \text{for } x = x_2 + w \quad (2.26)$$

$$\Delta p_3(x) = \Delta p_4(x) \quad \text{for } x = x_3 \quad (2.27)$$

$$D_{p_3} \frac{d\Delta p_3}{dx} = D_{p_4} \frac{d\Delta p_4}{dx} \quad \text{for } x = x_3 \quad (2.28)$$

$$D_{p_4} \frac{d\Delta p_4}{dx} = -S_{p_4} \Delta p_4 \quad \text{for } x = H \quad (2.29)$$

From equations (2.22), (2.24) and the boundary conditions, we obtain the following matrix system:

$$\begin{bmatrix} X_{11} & X_{12} & 0 & 0 \\ X_{21} & X_{22} & X_{23} & X_{24} \\ X_{31} & X_{32} & X_{33} & X_{34} \\ 0 & 0 & X_{43} & X_{44} \end{bmatrix} \begin{bmatrix} A'_3 \\ B'_3 \\ A'_4 \\ B'_4 \end{bmatrix} = \begin{bmatrix} X'_1 \\ X'_2 \\ X'_3 \\ X'_4 \end{bmatrix} \quad (2.30)$$

with :

$$\begin{aligned} X_{11} &= e^{-\frac{x_2+w}{L_{p3}}}; X_{12} = e^{-\frac{x_2+w}{L_{p3}}}; X_{21} = e^{-\frac{x_3}{L_{p3}}}; X_{22} = e^{-\frac{x_3}{L_{p3}}}; \\ X_{23} &= -e^{-\frac{x_3}{L_{p4}}}; X_{24} = -e^{-\frac{x_3}{L_{p4}}}; \\ X_{31} &= -\frac{D_{p3}}{L_{p3}} e^{-\frac{x_3}{L_{p3}}}; X_{32} = \frac{D_{p3}}{L_{p3}} e^{-\frac{x_3}{L_{p3}}}; X_{33} = \frac{D_{p4}}{L_{p4}} e^{-\frac{x_3}{L_{p4}}}; X_{34} = \\ & -\frac{D_{p4}}{L_{p4}} e^{-\frac{x_3}{L_{p4}}}; \\ X_{43} &= -e^{-\frac{H}{L_{p4}}} \left( \frac{D_{p4}}{L_{p4}} + S_{p4} \right); X_{44} = e^{-\frac{H}{L_{p4}}} \left( \frac{D_{p4}}{L_{p4}} - S_{p4} \right); \\ X'_1 &= \frac{\alpha_3 L_{p3}^2 F(1-R) e^{-\alpha_2(x_2+w_1)}}{D_{p3}(\alpha_3^2 L_{p3}^2 - 1)}; \\ X'_2 &= F(1-R) e^{[(\alpha_3-\alpha_2)(x_2+w_1)]} e^{-\alpha_3 x_3} \times \left[ \frac{\alpha_3 L_{p3}^2}{D_{p3}(\alpha_3^2 L_{p3}^2 - 1)} - \right. \\ & \left. \frac{\alpha_4 L_{p4}^2}{D_{p4}(\alpha_4^2 L_{p4}^2 - 1)} \right]; \\ X'_3 &= F(1-R) e^{[(\alpha_3-\alpha_2)(x_2+w_1)]} e^{-\alpha_3 x_3} \times \left[ \frac{\alpha_3^2 L_{p3}^2}{(\alpha_3^2 L_{p3}^2 - 1)} - \frac{\alpha_4^2 L_{p4}^2}{(\alpha_4^2 L_{p4}^2 - 1)} \right]; \\ X'_4 &= \frac{-\alpha_4 L_{p4}^2 F(1-R) e^{[(\alpha_3-\alpha_2)(x_2+w_1)]} e^{[(\alpha_4-\alpha_3)x_3]}}{D_{p4}(\alpha_4^2 L_{p4}^2 - 1)} \times e^{-\alpha_4 H} [S_{p4} - D_{p4} \alpha_4] \end{aligned}$$

The constants are determined using the Gauss algorithm [25]. The expression of the holes photocurrent is given by :

$$\begin{aligned} J_{p3}(x_2+w) &= -qD_{p3} \left[ \frac{A'_3}{L_{p3}} e^{(x_2+w)/L_{p3}} - \frac{B'_3}{L_{p3}} e^{-(x_2+w)/L_{p3}} - \right. \\ & \left. \alpha_3 K'_{p3} e^{-\alpha_3(x_2+w)} \right] \quad (2.31) \end{aligned}$$

### Calculation of result photocurrent

The photocurrent results from the contribution of the different areas of the structure. The recombinations of the photocarriers in the space charge region are neglected, then it can be written as [9]:

$$J_{ph} = J_{n_2}(x_2) + J_{n_{w_1}} + J_{n_{w_2}} + J_{p_3}(x_2+w) \quad (2.32)$$

The internal quantum efficiency is given by :

$$\eta = \left| \frac{J_{ph}}{J_0} \right| \quad (2.33)$$

with  $J_0 = qF(1-R)$  [26]. It is an arbitrary unit.

## Results and Discussion

In this part we present a result of different theoretical models developed by studying the effects of different geometrical parameters on the internal quantum efficiency. We compare the different results for each structure. We use  $H_i$  as the thickness of the region  $i$ .

### Homojunction: $\text{CuInSe}_2(p)/\text{CuInSe}_2(n)$ (Region 2/Region 3)

Study of the effect of front parameters

The figures 6 a), b), c) respectively show the effects of the thickness of the front layer, of the diffusion length and of the space charge region. The figure 6 d) gives the contribution of the different regions in the case of a thin thickness of the front layer. The surface recombination velocity is estimated at  $S_{n_2} = 2 \times 10^7 \text{ cm.s}^{-1}$  for including the effects of the losses of carriers by recombination at the surface of the front layer. It is noted that in

Figure 6 a) the internal quantum efficiency decreases when the thickness of the front increases. This can be explained partly by the fact that when the thickness of the front increases the majority of the photons are absorbed by the front layer. Few photons arrive in the rear areas. The recombination velocity at the front surface being high, which causes many losses carriers on the front surface by recombination phenomenon.

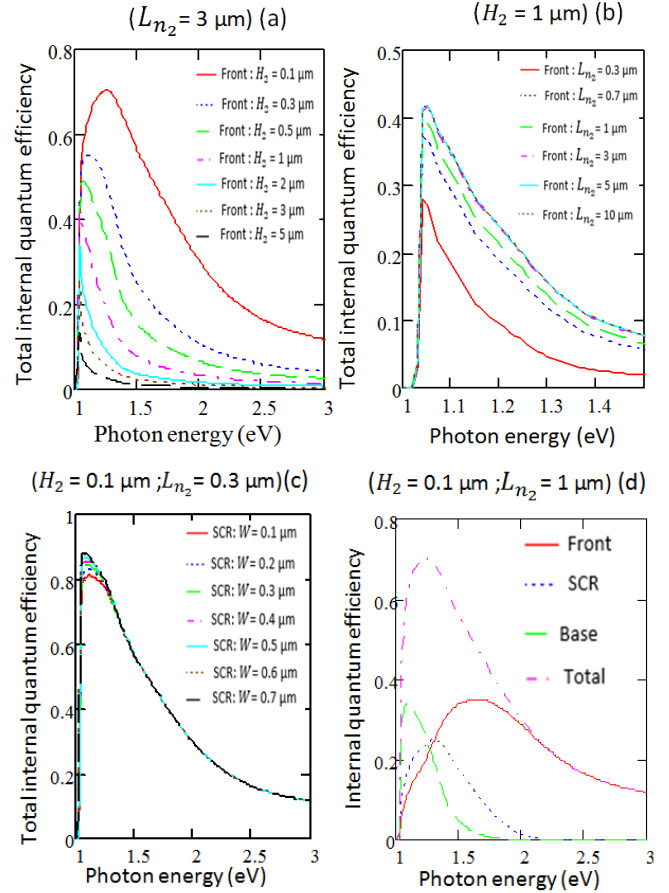


**Figure 6:** Internal quantum efficiency vs. Photon energy: a) effect of the front thickness; b) Effect of the diffusion length in the front; c) Effect of the thickness of the space charge region; d) contribution of the different regions. ( $S_{n_2} = 2 \times 10^7 \text{ cm.s}^{-1}$ ;  $S_{p_3} = 2 \times 10^7 \text{ cm.s}^{-1}$ ;  $L_{p_3} = 0.5 \mu\text{m}$ ;  $W = 0.1 \mu\text{m}$  (a; b and d))

On Figure 6 b) we study the effect of the diffusion length and fixed the front thickness at  $1 \mu\text{m}$ , allowing it to absorb most of the photons. The diffusion length varying from  $0.3$  to  $10 \mu\text{m}$  (doping level type  $p$  in range  $[10^{14}; 10^{20} \text{ cm}^{-3}]$ ). For the diffusion lengths less than the thickness of the front ( $L_{n_2} < H_2$ ) the internal quantum efficiency falls down, for those which are superior ( $L_{n_2} > H_2$ ) it always remains low, his maximum value is less than 45 %. The elevated losses of carriers on the front surface affect the influence of the diffusion length. Figure 6 c) we show the effect of the back areas (space charge region, base) by varying the thickness of the space charge region from  $0.1$  to  $0.7 \mu\text{m}$ , we evaluated the diffusion length in the base  $L_{p_3}$  at  $2.5 \mu\text{m}$ , the front thickness being fixed at  $0.1 \mu\text{m}$ . We observe a significant enhancement of the internal quantum efficiency, his maximum value passes above 80% in the range of low energies ( $1.04 < E < 1.2 \text{ eV}$ ). We also note that a variation of the thickness of the depletion region involves a weak variation of the signal; this effect can be explained by the

significant contribution of the base. For energies values greater than 1.4 eV the internal quantum efficiency gradually decreases and modeling a considerable absorption of the photons by the front layer. This phenomenon is illustrated in Figure 6 d) where the contribution of each region is highlighted.

**Homojunction with window layer: CuInS<sub>2</sub>(p<sup>+</sup>)/CuInSe<sub>2</sub>(p)/CuInSe<sub>2</sub>(n)  
(Region 1 / Region 2 / Region 3)**

*Study of the effect of region 2 parameters*

On Figure 7 a) we study the effect of the thickness of the second region. The diffusion length  $L_{n_2}$  is fixed at 3  $\mu\text{m}$ , the recombination velocity at the interface  $S_{n_2}$  is estimated at  $2 \times 10^3 \text{ cm.s}^{-1}$ . We note a good enhancement of the internal quantum efficiency. For the radiation energies lower than the CuInS<sub>2</sub> energy band gap but greater than the CuInSe<sub>2</sub> energy band gap, the internal quantum efficiency varies from 80 to 100% for a range of thicknesses values from 0.1 to 1  $\mu\text{m}$ , from 80 to 60% for thicknesses values in range from 2 to 3  $\mu\text{m}$ , and less than 60% for thicknesses values greater than the diffusion length.

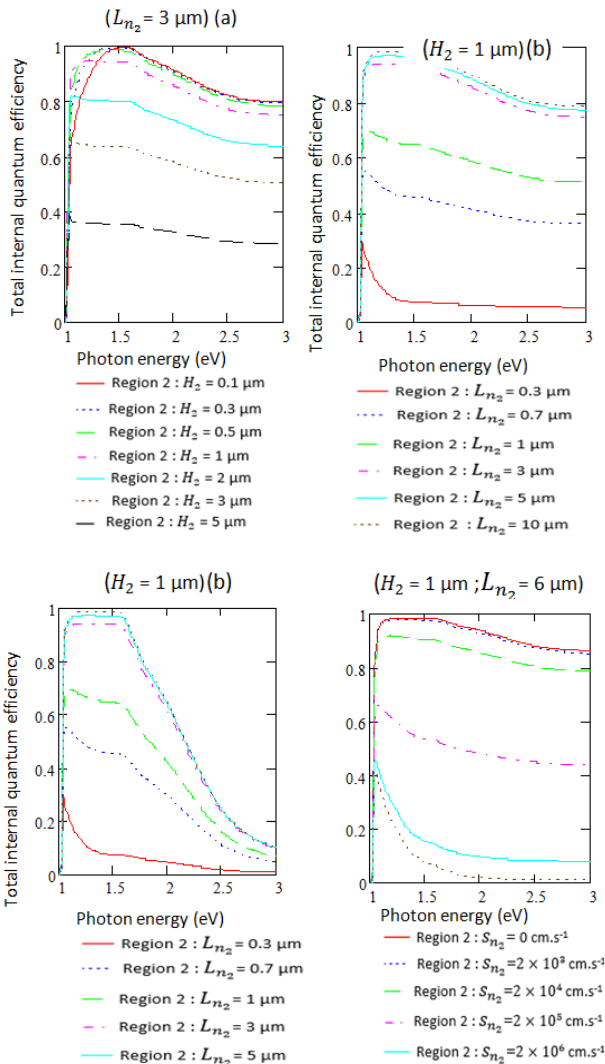
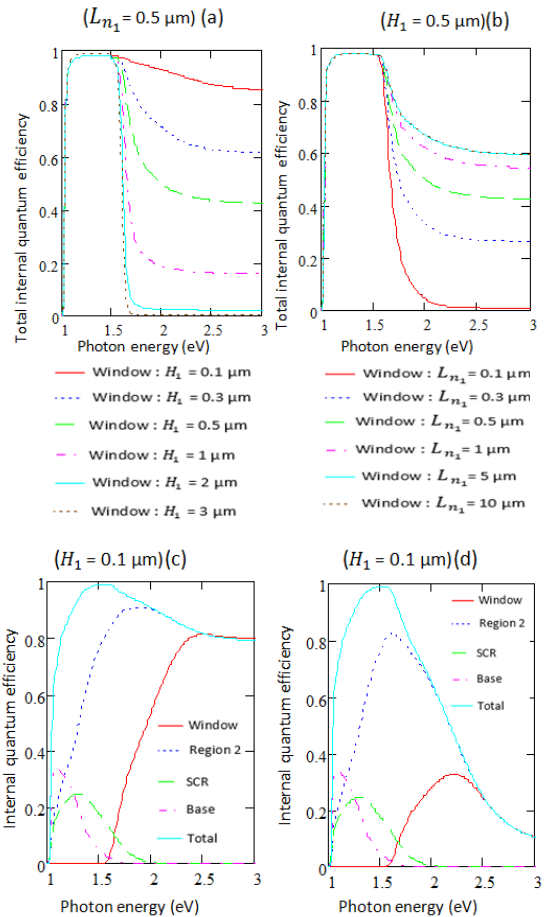


**Figure 7:** Internal quantum efficiency vs. Photon energy: a) effect of the region 2 thickness; b and c) effect of the diffusion length in region 2; d) effect of the recombination velocity at the interface window layer – region 2. ( $s_{n_1} = 2 \times 10^5 \text{ cm.s}^{-1}$  (a; b and d) and  $2 \times 10^7 \text{ cm.s}^{-1}$  (c);  $H_1 = 0.1 \mu\text{m}$ ;  $L_{n_1} = 0.2 \mu\text{m}$  (a; b and c) and  $0.5 \mu\text{m}$  (d);  $s_{n_2} = 2 \times 10^3 \text{ cm.s}^{-1}$  (a; b and c);  $s_{p_3} = 2 \times 10^7 \text{ cm.s}^{-1}$ ;  $L_{p_3} = 0.5 \mu\text{m}$ ;  $W = 0.1 \mu\text{m}$ ;  $H = 100 \mu\text{m}$ )

Figure 7 b) shows the effects of the diffusion length  $L_{n_2}$ , for the thickness of region 2 fixed at  $H_2 = 1 \mu\text{m}$ . We observe a considerable influence of the diffusion length on the internal quantum efficiency. This is due to the fact that losses carriers at the interface are minimized by the presence of the window layer ( $S_{n_2} = 2 \times 10^3 \text{ cm.s}^{-1}$ ).

For this thickness ( $H_2 = 1 \mu\text{m}$ ), a diffusion length  $L_{n_2}$  greater than 3  $\mu\text{m}$  is sufficient to obtain the best response. For values of  $L_{n_2}$  much lower than  $H_2$  the internal quantum efficiency is low. The figure 7 c) shows the effects of losses carriers in the window layer ( $S_{n_1} = 2 \times 10^7 \text{ cm.s}^{-1}$ ) causing a low signal of the internal quantum efficiency for the energies values greater than the energy band gap of the window layer ( $E > 1.57 \text{ eV}$ ). On Figure 7 d) we study the effect of the recombination velocity at the interface, we fixed  $H_2 = 1 \mu\text{m}$  and  $L_{n_2} = 6 \mu\text{m}$ , losses of carriers by recombination at the interface remain low for recombination velocity  $S_{n_2}$  lower than  $2 \times 10^3 \text{ cm.s}^{-1}$ . For  $S_{n_2}$  values ranging from  $2 \times 10^3$  to  $2 \times 10^5 \text{ cm.s}^{-1}$  the losses of carriers by recombination become significant and affect the internal quantum efficiency. For those that are greater than  $2 \times 10^6 \text{ cm.s}^{-1}$  the effects of the losses of carriers by recombination at the interface are important and the internal quantum efficiency decreases despite of the high value of the diffusion length ( $L_{n_2} = 6 \mu\text{m}$ ).

*Effect of the Window layer*



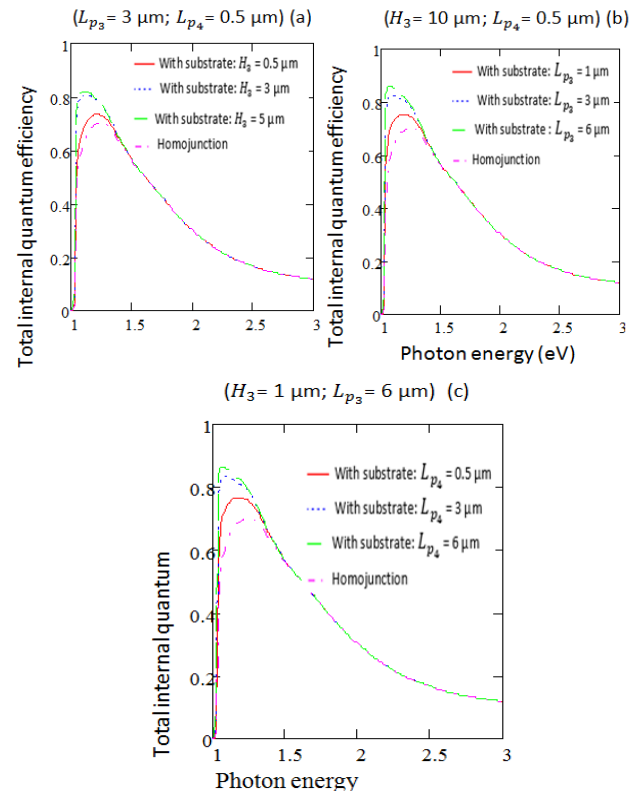
**Figure 8:** Internal quantum efficiency vs. Photon energy: a) effect of the window thickness; b) Effect of the diffusion length in the window; c and d) contribution of the different regions ( $s_{n_1} = 2 \times 10^5 \text{ cm.s}^{-1}$  (a; b and c) and  $2 \times 10^7 \text{ cm.s}^{-1}$  (d);  $H_1 = 0.1 \mu\text{m}$  (c and d);  $L_{n_1} = 0.2 \mu\text{m}$  (c and d);  $H_2 = 1 \mu\text{m}$  (a and b) and  $0.1 \mu\text{m}$  (c and d);  $L_{n_2} = 6 \mu\text{m}$  (a and b) and  $1 \mu\text{m}$  (c and d);  $s_{n_2} = 2 \times 10^3 \text{ cm.s}^{-1}$ ;  $s_{p_3} = 2 \times 10^7 \text{ cm.s}^{-1}$ ;  $L_{p_3} = 0.5 \mu\text{m}$ ;  $W = 0.1 \mu\text{m}$ ;  $H = 100 \mu\text{m}$ )

Figure 8 a) shows the effect of the thickness of the window layer. The interest is to decrease the thickness of the window layer to increase the photon number that reach the region 2 and enhance the signal at the photon energies greater than the CuInSe<sub>2</sub> energy band gap. Figure 8 b) shows the effect of the diffusion length in the window layer. The contribution of the window layer to the quantum internal efficiency depend of the diffusion length. His contribution is more important if the diffusion length increases. We also note that despite of a high value of the diffusion length ( $L_{n1} > 5 \mu\text{m}$ ) a thin thickness of the window layer is sufficient. The Figures 8 c) and 8 d) show the effects of these losses of carriers for radiation energies greater than the energy band gap of the window layer ( $E > 1.57 \text{ eV}$ ). The Figure 8 c) we fixed  $S_{n1} = 2 \times 10^5 \text{ cm.s}^{-1}$  and we observe a shallow decrease of the internal quantum efficiency. On Figure 8 d) the recombination velocity at the surface is more elevated, we fixed  $S_{n1} = 2 \times 10^7 \text{ cm.s}^{-1}$  and we observe an important decrease of the signal.

#### Homojunction deposited on substrate: CuInSe<sub>2</sub>(p)/CuInSe<sub>2</sub>(n)/CuInSe<sub>2</sub>(n<sup>+</sup>)(Region 2/Region 3/Region 4)

##### Base and Substrate effects

On figures 9 the effects of the base and substrate are studied. We note their effects only in the range of low photons energies ( $E < 1.4 \text{ eV}$ ). For elevated energies ( $E > 1.5 \text{ eV}$ ), most of the photons are absorbed in the front areas (region 2 and the space charge region). We also assume that the presence of the substrate will permit to increase the purity of the base by reducing the level of doping in this region ( $n < 10^{16} \text{ cm}^{-3}$ ) in order to increase the diffusion length ( $L_{p3} > 3 \mu\text{m}$ ) compared to the homojunction or the homojunction with window layer ( $L_{p3} < 0.5 \mu\text{m}$ ). The level of doping in the substrate being higher ( $n > 10^{16} \text{ cm}^{-3}$ ).



**Figure 9** : Internal quantum efficiency vs. Photon energy: a) effect of the base thickness; b) Effect of the diffusion length in the base; c) Effect of the diffusion length in the substrate ( $H_2 = 0.1 \mu\text{m}$ ;  $L_{n2} = 3 \mu\text{m}$ ;  $s_{n2} = 2 \times 10^7 \text{ cm.s}^{-1}$ ;  $s_{p4} = 2 \times 10^7 \text{ cm.s}^{-1}$ ;  $W = 0.1 \mu\text{m}$ ;  $H = 100 \mu\text{m}$ ); Homojunction :  $L_{p3} = 0.5 \mu\text{m}$ ;  $s_{p3} = 2 \times 10^7 \text{ cm.s}^{-1}$ )

Figure 9 a) shows the influence of the thickness of the base on the internal quantum efficiency. We fixed the diffusion length  $L_{p3} = 3 \mu\text{m}$ . For thicknesses values less than  $L_{p3}$  the spectral response increases with the thickness. For those which are greater or equal at  $L_{p3}$ , the internal quantum efficiency is identical. Figure 9 b) confirms this report by studying the effect of the diffusion length, the thickness of the base is fixed at  $H_3 = 10 \mu\text{m}$ , the internal quantum efficiency increases with the diffusion length,  $L_{p3}$  varying from 1 to 6  $\mu\text{m}$ . On figure 9 c), we study the contribution of the substrate to the internal quantum efficiency. For this, we have reduced the thickness of the base at 1  $\mu\text{m}$  allowing the photons to reach the substrate. The substrate contributes to the enhancement of the internal quantum efficiency as well as the base. An increase diffusion length  $L_{p4}$  in the substrate causes an increase of the spectral response.

#### Comparative study of homojunction deposited on substrate (p/n/n<sup>+</sup>) to homojunction (p/n) and homojunction with window layer (p<sup>+</sup>/p/n)

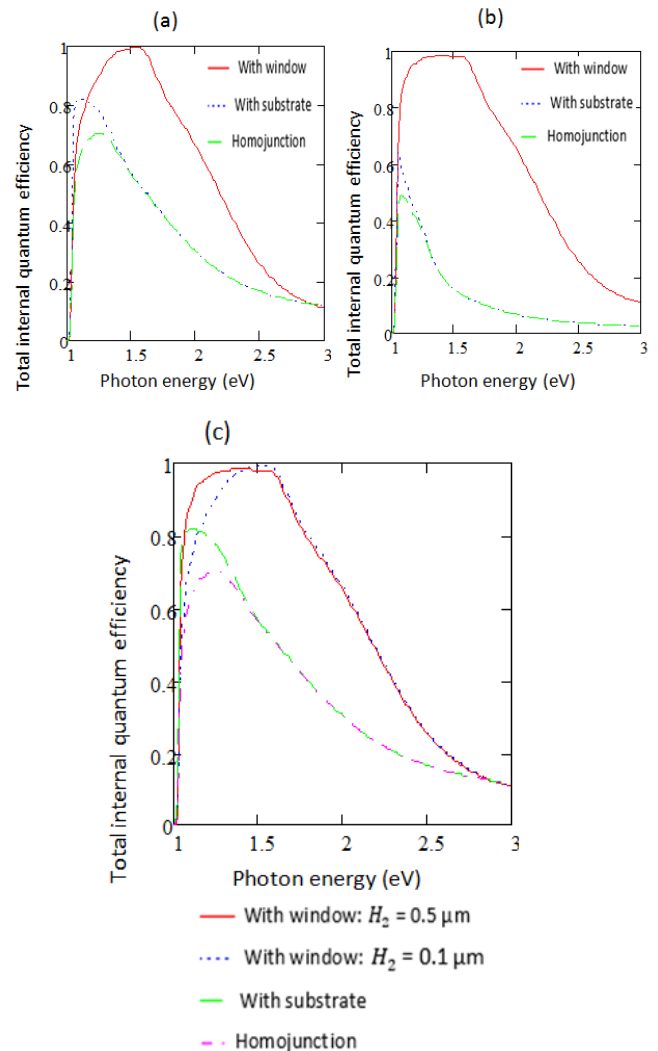


**Figure 10**: Internal quantum efficiency vs. Photon energy: Comparative Study of the different models. ( $s_{n1} = 2 \times 10^7 \text{ cm.s}^{-1}$ ;  $H_1 = 0.1 \mu\text{m}$ ;  $L_{n1} = 0.5 \mu\text{m}$ ;  $H_2 = 0.1 \mu\text{m}$  (a) ; c : homojunction and homojunction with substrate) and  $0.5 \mu\text{m}$  (b) ;  $L_{n2} = 3 \mu\text{m}$ ;  $s_{n2} = 2 \times 10^3 \text{ cm.s}^{-1}$  (homojunction with window) and  $2 \times 10^7 \text{ cm.s}^{-1}$  (homojunction and homojunction with substrate) ;  $s_{p3} = 2 \times 10^7 \text{ cm.s}^{-1}$  (homojunction) ;  $L_{p3} = 3 \mu\text{m}$  and  $0.5 \mu\text{m}$  (Homojunction) ;  $H_3 = 5 \mu\text{m}$  ;  $s_{p4} = 2 \times 10^7 \text{ cm.s}^{-1}$  ;  $L_{p4} = 0.5 \mu\text{m}$ ;  $W = 0.1 \mu\text{m}$ ;  $H = 100 \mu\text{m}$ )

On Figure 10 a) we compare the three models studied. The thickness of the region 2 is fixed at 0.1  $\mu\text{m}$ . For the homo junction deposited on substrate (CuInSe<sub>2</sub>(p)/CuInSe<sub>2</sub>(n)/CuInSe<sub>2</sub>(n<sup>+</sup>)) we note the effect of the substrate for the energy values less than 1.4 eV. For energy values greater than 1.4 eV, the internal quantum efficiency is identical to the homo junction (CuInSe<sub>2</sub>(p)/CuInSe<sub>2</sub>(n)) response. So the photons do not access the substrate for this energy range. We also note that the homo junction deposited on substrate dominates the spectral response on a very small range of photon energies ( $E < 1.2$  eV), otherwise the model of the homo junction with window layer (CuInSe<sub>2</sub>(p+)/CuInSe<sub>2</sub>(p)/CuInSe<sub>2</sub>(n)) gives the best signal. On Figure 10 b), we increased the thickness of the second region at 0.5  $\mu\text{m}$ . We observe an enhancement of the internal quantum efficiency for the model type CuInSe<sub>2</sub>(p+)/CuInSe<sub>2</sub>(p)/CuInSe<sub>2</sub>(n) caused by the effect of the window layer. The losses of recombination carriers at the interface between the window layer and the second region are reduced ( $S_{n_2} = 2 \times 10^3 \text{cm} \cdot \text{s}^{-1}$ ). We also note a decrease of the internal quantum efficiency in the case of the structures types CuInSe<sub>2</sub>(p)/CuInSe<sub>2</sub>(n)/ CuInSe<sub>2</sub>(n<sup>+</sup>) and CuInSe<sub>2</sub>(p)/CuInSe<sub>2</sub>(n) caused by the heavy losses of recombination carriers observed on the front surface (no window layer:  $S_{n_2} = 2 \times 10^7 \text{cm} \cdot \text{s}^{-1}$ ). On Figure 10 c) we compare the spectral responses obtained on Figure 10-a) and that obtained on Figure 10 b) for the model CuInSe<sub>2</sub>(p+)/CuInSe<sub>2</sub>(p)/CuInSe<sub>2</sub>(n). It shows the importance of the window layer, the homo junction with window layer (CuInSe<sub>2</sub>(p+)/CuInSe<sub>2</sub>(p)/CuInSe<sub>2</sub>(n)) gives the best signal followed by the homo junction deposited on substrate (CuInSe<sub>2</sub>(p)/CuInSe<sub>2</sub>(n)/ CuInSe<sub>2</sub>(n<sup>+</sup>)). The homo junction (CuInSe<sub>2</sub>(p)/CuInSe<sub>2</sub>(n)) gives the low signal. The decrease of the signal observed in the range of elevated energies ( $E > 1.57$  eV) on each graph is due by the losses of carriers by recombination caused by the dislocation of the surface in the front layer (illuminated surface).

## Conclusions

In this work we have studied the internal quantum efficiency of solar cells based on CuInSe<sub>2</sub>. We have developed a theoretical models for three layers. We have done a theoretical simulation on all spectral responses studied by variation of physical parameters ( $L_n$ ,  $L_p$ ,  $S_n$ ,  $S_p$ , ...) in order to enhance performances of the device. For the two layers model (p/n) we considered the homo junction type CuInSe<sub>2</sub>(p)/CuInSe<sub>2</sub>(n), we took into account the losses of recombination carriers on the front surface. These losses carriers affect the influence of the diffusion length and provoke a considerable decrease of the internal quantum efficiency. The effects of these losses carriers can be minimized by reducing the contribution of the front layer. This is possible by realizing the junction near the surface (shallow junction) or replacing the front layer by a wide gap window layer (structure n/P type: CdS(n)/CuInSe<sub>2</sub>(p), ZnO(n)/CdS(n)/CuInSe<sub>2</sub>(p)). The deposit of a window layer based on CuInSe<sub>2</sub> on the front layer (CuInSe<sub>2</sub>(p<sup>+</sup>)/CuInSe<sub>2</sub>(p)/CuInSe<sub>2</sub>(n)) can reduce the recombination of the carriers at the front surface observed in the case of the homo junction. It provokes a considerable increase of the internal quantum efficiency for photon energies lower than the energy band gap of the CuInSe<sub>2</sub> window layer ( $1.04 < E < 1.57$  eV). For the homo junction model, the presence of a wide substrate enhances the internal quantum efficiency for the radiation of low energies range [1.04 ; 1.4 eV] corresponding to a low absorption coefficients of the different layers. Our best theoretical internal quantum efficiency is obtained with the model CuInSe<sub>2</sub>(p<sup>+</sup>)/CuInSe<sub>2</sub>(p)/CuInSe<sub>2</sub>(n) (homo junction with window layer).

The presence of the window layer allows to reduce considerably the recombination velocity of the surface. This effect allows to increase considerably the internal quantum efficiency for photon energies lower than the gap of the CuInSe<sub>2</sub> (1.57 eV). We note that, for photon energies greater than the gap of the CuInSe<sub>2</sub> (1.57 eV), the signal disappears for a thickness of the window layer greater than 2  $\mu\text{m}$ .

## Nomenclature :

$\beta$  :  $n$  (electrons) or  $p$  (holes) ;  $i$  : region (1, 2 ou 3)

$\alpha_i$  : Absorption coefficient of region  $i$  ( $\text{cm}^{-1}$ )

$F$  : Incident photons flux ( $\text{cm}^{-2} \cdot \text{s}^{-1}$ )

$R$  : Reflection coefficient

$\tau_{\beta_i}$  : Lifetime of free electrons or holes photocreated in region  $i$  ( $\mu\text{s}$ )

$\Delta\beta_i(x)$  : Density of free electrons or holes photocreated in region  $i$  at the point of  $x$  coordinate ( $\text{cm}^{-3}$ )

$J_{\beta_i}(x)$  : Photocurrent density of free electrons or holes photocreated in region  $i$  at the point of  $x$  coordinate ( $\text{A} \cdot \text{cm}^{-2}$ )

$J_{ph}$  : Total density of photocurrent ( $\text{A} \cdot \text{cm}^{-2}$ )

$D_{\beta_i}$  : Diffusion coefficient of free electrons or holes photocreated in region  $i$  ( $\text{cm}^2 \cdot \text{s}^{-1}$ ) ( $D_{n_1} = D_{n_2} = 15.41 \text{cm}^2 \cdot \text{s}^{-1}$  and  $D_{p_3} = D_{p_4} = 1.28 \text{cm}^2 \cdot \text{s}^{-1}$ )

$L_{\beta_i}$  : Diffusion length of free electrons or holes photocreated in region  $i$  ( $\mu\text{m}$ )

$S_{\beta_i}$  : Recombination velocity on the surface (or to the interface) of region  $i$  ( $\text{cm} \cdot \text{s}^{-1}$ )

$H$  : Thickness of the structure ( $\mu\text{m}$ )

$H_i$  : Thickness of the region  $i$  ( $\mu\text{m}$ )

$w_i$  : Thickness of the region  $i$  of the space charge zone (SCZ) ( $\mu\text{m}$ )

$q$  : Elementary charge ( $1.6 \times 10^{-19} \text{C}$ )

## References

1. C.-H. Huang, "Effects of Ga content on Cu(In,Ga)Se<sub>2</sub> solar cells studied by numerical modeling", Journal of Physics and Chemistry of Solids 69 (2008) 330–334
2. O. Tesson, M. Morsli, A. Bonnet, V. Jousseume, L. Cattin, G. Massé, "Electrical characterisation of CuInSe<sub>2</sub> thin films for solar cells applications", Optical Materials, 9(1998) 511.
3. B. Eisener, M. Wagner, D. Wolf, G. Muller, "Study of the intrinsic defects in solution grown CuInSe<sub>2</sub> crystals depending on the path of crystallization", J. Cryst Growth, 198-199 (1999) 321.
4. C.J. Huang et al., "Formation of CuInSe<sub>2</sub> thin films on flexible substrates by electrodeposition (ED) technique", Solar Energy Materials & Solar Cells 82 (2004) 553–565
5. S. MEHDAOUI, O. AISSAOUI, N. BENSLIM, M. BENABDESLEEM, L. BECHIRI et L. MAHDJOURI, "ELABORATION ET ETUDE DES MATERIAUX CHALCOPYRITES A B<sup>III</sup>C<sub>2</sub><sup>IV</sup> : LE DISELINURE DE CUIVRE ET D'INDIUM", Sciences & Technologie A – N°25, Juin. (2007), pp. 15-18
6. O. Meglali et al., "Characterization of CuInSe<sub>2</sub> thin films elaborated by electrochemical deposition", Revue des Energies Renouvelables Vol. 11 N°1 (2008) 19 – 24.
7. J.H. Schon, E. Arushanov, Ch. Kloc, and E. Bucher, "Electrical and photoluminescence properties of CuInSe<sub>2</sub> single crystals", J. Appl. Phys. 81; 6205 (1997).
8. M. V. Yakushev, a. v. Mudryi, V. F. Gremenok, E. P. Zaretskaya, V. B. Zaleski, Y. Feofanov, R. W. Martin, "Influence of growth conditions on the structural quality of Cu(InGa)Se<sub>2</sub> and CuInSe<sub>2</sub> thin films", Thin. Solid. Films 451-452 (2004) 133-136
9. Henry Mathieu, cours, "physique des semiconducteurs et des composants électroniques", 2001, 5<sup>e</sup> édition, DUNOD, p. 124.

10. S. Khelifi et A. Belghachi, "Le Rôle de la Couche Fenêtre dans les Performances d'une Cellule Solaire GaAs", *Rev. Energ. Ren.* Vol.7 (2004)13-21.
11. SubbaRamaiahKodigala, "Cu(In<sub>1-x</sub>Ga<sub>x</sub>)se<sub>2</sub>based thin solar cells", 2010, Volume 35, Academic Press, ELSEVIER.Inc, p. 16.
12. J.L. Shay, J.H. Wernick: "Ternary chalcopyrite semiconductors: growth, electronic properties, and applications", Chapter 2: "The chalcopyrite structure and crystal growth", pp. 3-78, Pergamon Press, Oxford, New York, Toronto, Sydney, Paris, Braunschweig (1975)
13. T. Loher, W. Jaegermann, C. Pettenkofer, "Formation and electronic properties of the CdS/CuInSe<sub>2</sub> (011) heterointerface studied by synchrotron-induced photoemission", *J. Appl. Phys.* 77 (1995) 731.
14. H. Hahn, G. Frank, W. Klinger, A.D. Meyer, G. Storger, "Über einigeternäreChalkogenidemitChalcopyritestruktur", *Z. Anorg. Aug. Chem.* 271 (1953) 153.
15. M. Robbins, V.G. Lambrecht Jr., "Preparation and some properties of materials in systems of the type M<sup>I</sup>M<sup>III</sup>S<sub>2</sub> / M<sup>I</sup>M<sup>III</sup>Se<sub>2</sub> where M<sup>I</sup> = Cu, Ag and M<sup>III</sup> = Al, Ga, In", *Mater. Res. Bull.* 8 (1973) 703.
16. I.V. Bodnar, B.V. Korzun, A.I. Lukomski, "Composition Dependence of the Band Gap of CuInS<sub>2x</sub>Se<sub>2(1-x)</sub>", *Phys. Stat. Solidi (B)* 105 (1981) K143.
17. S.J. Fonash, *Solar Cell device Physics*, Academic Press, New York, 1981.
18. H.L. Hwang, C.Y. Sun, C.Y. Leu, C.C. Cheng, C.C. Tu, "Growth of CuInS<sub>2</sub> and its characterization", *Rev. Phys. Appl.* 13 (1978) 745.
19. R. L. Anderson, "Germanium-gallium arsenide heterojunctions", *IBM J.Res.Dev.* 4, 283, 1960.
20. B. MBOU, A. MEZERREG, N. REZZOUG, and C.LLINARES, "Calculated and Measured Spectral Responses in Near-Infrared of III-V Photodetectors Based on Ga, In, and Sb", *phys. Stat. Sol. (a)* 141, 511 (1994).
21. H. J. HOVEL and J. M. WOODALL, "Ga<sub>1-x</sub>Al<sub>x</sub>As - GaAs P-P-N Heterojunction Solar Cells", *J. Electrochem. Soc.* 120, 1246 (1973).
22. H. J. HOVEL and J. M. WOODALL, 10th IEEE Photovoltaic Specialists Conf., Palo Alto (Calif.) 1973 (p.25).
23. A. LAUGIER and U. A. ROGER, *Les photopiles solaires*, Technique et Documentation, Paris 1981.
24. H. LUQUET, L. GOUSKOV, M. PEROTIN, A. JEAN, A. RJEB, T. ZAROURI, and G. BOUGNOT, "Liquid- phase-epitaxial growth of Ga<sub>0.96</sub>Al<sub>0.04</sub>Sb: Electrical and photoelectrical characterizations", *J. appl. Phys.* 60, 3582 (1986).
25. Michelle Schatzman, *cours et exercices, analyse numerique, Une approche mathematique*, 2001, 2<sup>e</sup> édition, DUNOD, p.211.
26. H. J. HOVEL, "Semiconductors and Semimetals: Solar Cells", 11, Academic Press, New York, 127 (1975).

